ACS OMEGA

http://pubs.acs.org/journal/acsodf

Article

Atomic-Scale Resolution Insights into Structural and Dynamic Differences between Ofloxacin and Levofloxacin

Bijay Laxmi Pradhan, Jai Prakash Yadav, Lekhan Lodhi, Prince Sen, Krishna Kishor Dey,* and Manasi Ghosh*

Cite This: *ACS Omega* 2023, 8, 24093−24105

Read Online

ACCESS | Metrics & More | Article Recommendations | Supporting Information

ABSTRACT: This study employs advanced solid-state NMR techniques to investigate the atomic-level structure and dynamics of two enantiomers: ofloxacin and levofloxacin. The investigation focuses on critical attributes, such as the principal components of the chemical shift anisotropy (CSA) tensor, the spatial proximity of ^{1}H and ^{13}C nuclei, and site-specific ^{13}C spin−lattice relaxation time, to reveal the local electronic environment surrounding specific nuclei. Levofloxacin, the levo-isomer of ofloxacin, exhibits higher antibiotic efficacy than its counterpart, and the dissimilarities in the CSA parameters indicate significant differences in the local electronic configuration and nuclear spin dynamics between the two enantiomers. Additionally, the study employs the $^{1}H-^{13}C$ frequency-switched Lee−Goldburg heteronuclear correlation (FSLGHETCOR) experiment to identify the presence of heteronuclear correlations between specific nuclei (C15 and H7 nuclei and C13 and H12 nuclei) in ofloxacin but not in levofloxacin. These observations offer insights into the link between bioavailability and nuclear spin dynamics, underscoring the significance of NMR crystallography approaches in advanced drug design.

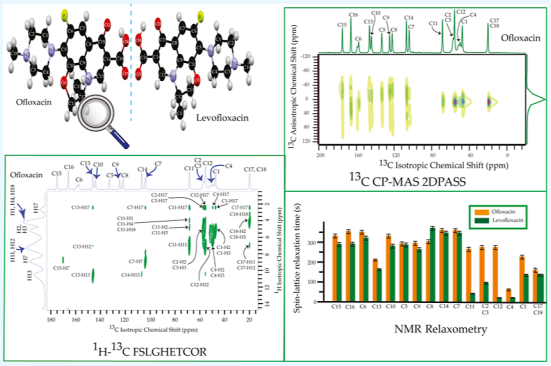

1. INTRODUCTION

The antibacterial class known as broad-spectrum fluoroquinolones functions by inhibiting two enzymes that are vital to bacterial DNA synthesis: topoisomerase and DNA gyrase.[1,2] Among the various fluoroquinolones, ofloxacin demonstrates the most robust activity owing to its oxazinoquinoline core consisting of three fused rings, including a fluoroquinolone ring and an oxazine ring. This ring has a methyl group that can exist in two optically active forms: *L*-isomer and *R*-isomer. Levofloxacin is the *L*-isomer, which is a chiral version of ofloxacin, and its antibacterial activity is higher than that of ofloxacin.[3−6] Despite the similarity in structure between the enantiomers, the arrangement of atoms, packing fraction, and *R*-factor percentages differ due to the distinct space groups and lattice points.[7] The aromatic and piperazine rings in both compounds are primarily planar and chair-conformational, respectively.[7−9] The structure of ofloxacin and levofloxacin is shown in Figure 1. The primary objective of this study is to develop and present a comprehensive and comparative NMR crystallography database for the fluoroquinolone antibiotics, ofloxacin and levofloxacin, with a particular focus on their atomic-level structures and dynamics. By providing a thorough understanding of the differences in the chemical environments and nuclear spin dynamics between these two isomers, this database will serve as a valuable resource for researchers and pharmaceutical scientists involved in the design and development of novel, more effective antibiotics. Through the use of advanced solid-state (SS) NMR techniques, this work aims to contribute to the advancement of drug design and facilitate the discovery of new antibiotics with improved efficacy and reduced toxicity.

SSNMR is an essential tool for determining the detailed structure and dynamics of drug molecules[10−19] and correlating motional dynamics with biological activity.[20,21] Studies have shown that ^{13}C nuclear spin dynamics are significantly affected by the substitution of various functional groups with the backbone of glucocorticoids.[21] Recent advancements in probe technology have revolutionized NMR spectroscopy of solids, enabling fast mechanical rotation of samples at frequencies exceeding 100 kHz. This breakthrough has unlocked a multitude of possibilities for the exploration of novel NMR techniques and their application in the study of various solid materials. These materials include globular and membrane-associated proteins, self-assembled protein aggregates like amyloid fibers, RNA, viral assemblies, polymorphic pharma-

Received: May 16, 2023
Accepted: June 9, 2023
Published: June 20, 2023

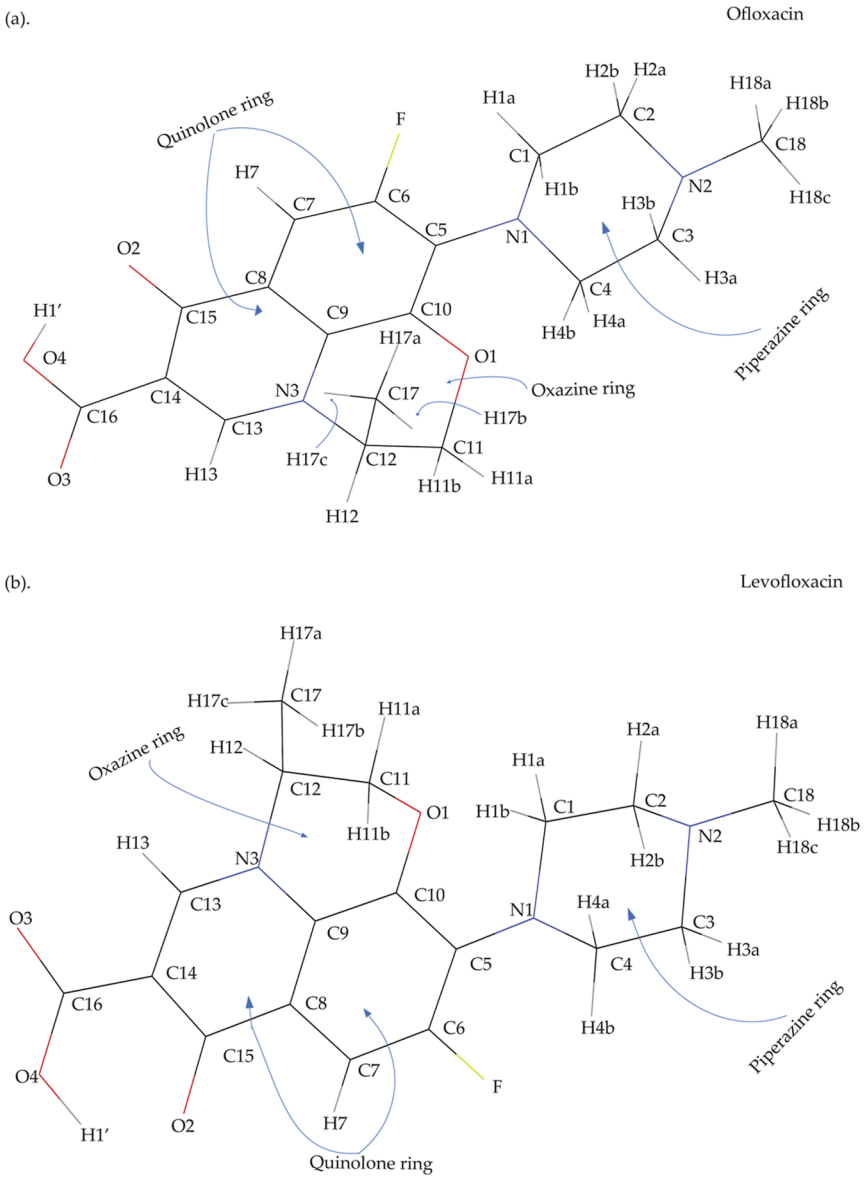

Figure 1. Structure of (a) ofloxacin and (b) levofloxacin.

ceuticals, metal−organic frameworks, bone materials, and inorganic substances. While the development of ultrafast-MAS (magic angle spinning) techniques is ongoing, several noteworthy advantages have emerged, such as the ability to handle minute sample quantities, reduced radio frequency requirements, shorter recycle delays for faster data acquisition, the feasibility of proton detection, improved proton spectral resolution, enhanced polarization transfer efficiency, and heightened sensitivity per unit sample. As ultrafast-MAS NMR techniques gain popularity in diverse research fields, efforts are being made concurrently to advance instrumentation, probes, and methodologies.[22,23] The spin−lattice relaxation time serves as a potent tool to investigate the spin-dynamics at each chemically unique nucleus site. In the case of ^{13}C nuclei, the spin−lattice relaxation process is predominantly influenced by chemical shift anisotropy (CSA) interactions and heteronuclear dipole−dipole interactions at high magnetic field values.[24−27] Consequently, CSA parameters furnish vital details regarding both the local electronic symmetry and the motional dynamics of the molecule. NMR crystallography can provide comprehensive structural and dynamic information about each crystallographically distinct nuclei site of polycrystalline and amorphous compounds, making it more sophisticated than X-ray crystallography. The CSA tensor is a crucial parameter for determining the local structure and conformation of a molecule, with the principal components of CSA parameters providing information about the local electronic structure, chemical bonding, and dynamics. The direction of the induced local magnetic field at a particular nuclear site depends on the symmetry of the electron distribution surrounding the nuclei and the spatial orientation of the molecule with respect to the external magnetic field.[28−39] Hence, determining the CSA tensor through high-resolution SSNMR experiments can generate comprehensive structural information about a molecule. Various SSNMR methodologies, such as two-dimensional MAS/CSA NMR experiment,[40] SUPER(separation of undistorted powder patterns by effortless recoupling),[41] ROCSA (recoupling of CSA),[42] RNCSA (γ-encoded R N_n^{ν}-symmetry based CSA),[43] 2DMAF (two-dimensional magic angle flipping),[44−46]

https://doi.org/10.1021/acsomega.3c03406
ACS Omega 2023, 8, 24093−24105

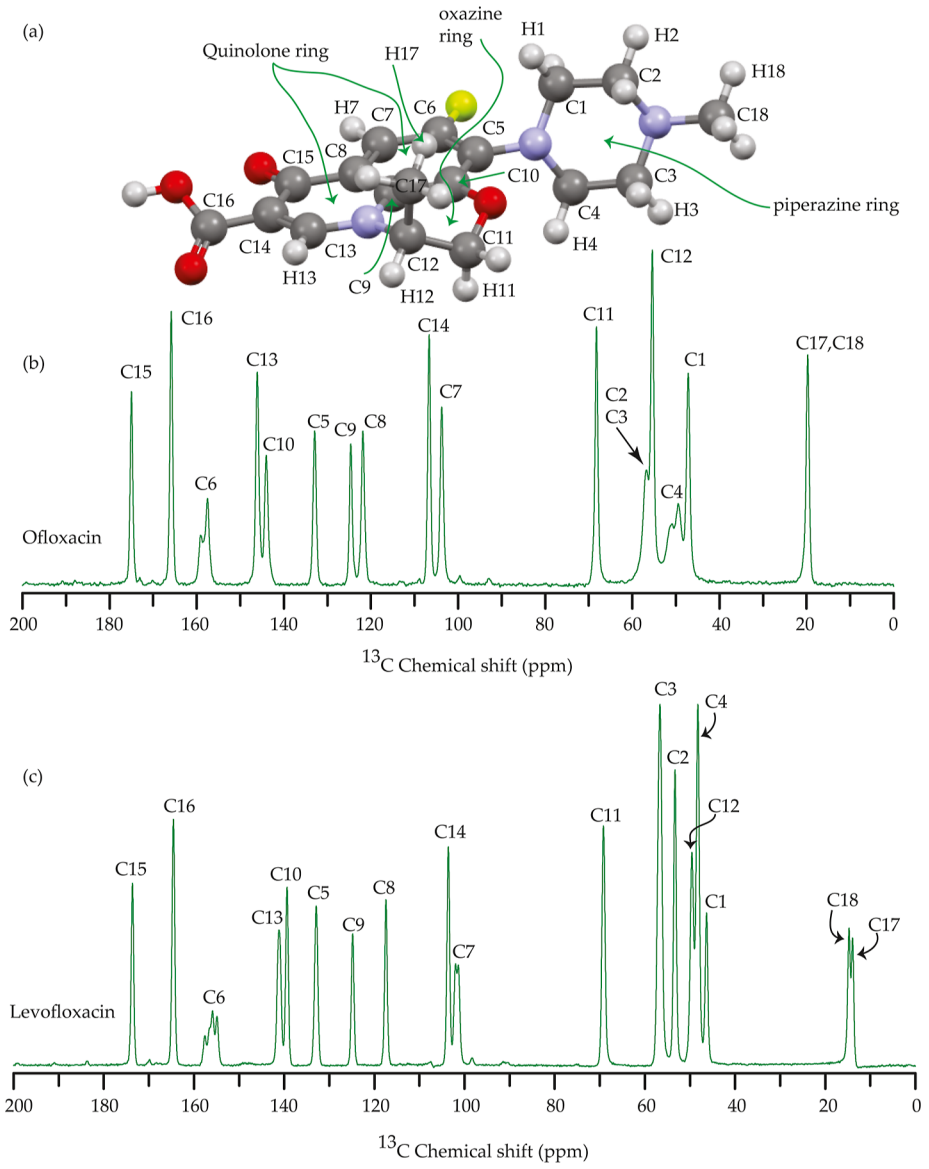

Figure 2. (a) Chemical structure of ofloxacin. ^{13}C CP-MAS spectrum of (b) ofloxacin and (c) levofloxacin at a MAS frequency of 10 kHz. The experiments were performed using a 500 MHz JEOL spectrometer with a contact time of 2 ms and a recycle delay of 15 s, and the number of scans was 2048.

2DMAT (two-dimensional magic angle turning),[47] and 2DPASS MAS (two-dimensional phase-adjusted spinning sideband magic angle spinning) SSNMR experiment,[48,49] can measure the CSA tensor and monitor changes in the local electronic distribution surrounding each chemically distinct carbon nucleus between ofloxacin and levofloxacin.

The ^{13}C 2DPASS CP-MAS SSNMR technique has been successfully applied to determine the principal components of CSA parameters in biopolymers,[50−55] drug molecules,[10−21] and co-crystals.[56]

2. EXPERIMENTAL SECTION

For this study, the active pharmaceutical ingredients (APIs) of both ofloxacin and levofloxacin were procured from Sigma-Aldrich. The experimental procedures involved the use of advanced NMR techniques such as ^{13}C CP-MAS SSNMR, ^{1}H−^{13}C FSLGHETCOR, and ^{19}F MAS SSNMR, which were performed using a Bruker Avance Neo 600 MHz NMR spectrometer equipped with a 3.2 mm double-resonance MAS probe. The MAS frequency used for ^{13}C CP-MAS SSNMR and ^{1}H−^{13}C FSLGHETCOR experiments was 10 kHz, while for ^{19}F MAS SSNMR, it was 24 kHz. Additionally, the ^{13}C spin−lattice relaxation time was measured using the method outlined by Torchia[57] on a JEOL ECX 500 MHz NMR spectrometer fitted with a 3.2 mm JEOL double-resonance MAS probe at a MAS frequency of 10 kHz. The specific conditions for the ^{13}C CP-MAS SSNMR experiment and spin−lattice relaxation experiment were previously discussed in a published article.[10,11]

^{1}H−^{13}C frequency-switched Lee−Goldburg heteronuclear correlation (FSLGHETCOR) experiment[58] is performed at a MAS frequency of 10 kHz. It is carried out with a 3.2 mm double-resonance probe with the 600 MHz Bruker Avance Neo instrument. The CP contact time was 200 μs. The FSLG homo-nuclear decoupling was used in the proton channel during t1 increments, and the block size of the FSLG pulse was 10 μs which is very small compared to the MAS period. During acquisition, TPPM hetero-nuclear decoupling was used. The

https://doi.org/10.1021/acsomega.3c03406
ACS Omega 2023, 8, 24093−24105

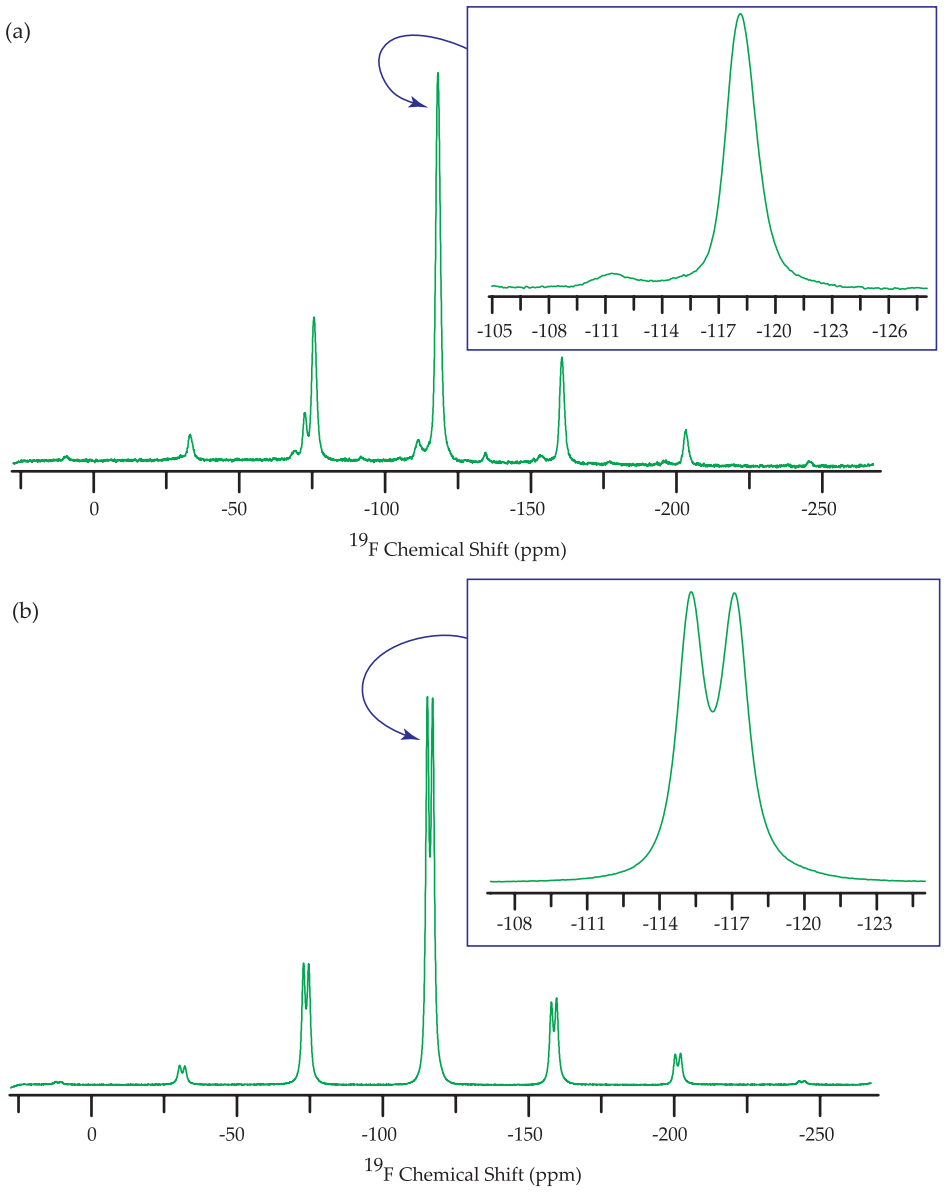

Figure 3. ^{19}F MAS SSNMR spectrum of (a) ofloxacin and (b) levofloxacin. The experiments were performed using a 600 MHz Bruker Avance Neo spectrometer with a recycle delay of 10 s, and the number of scans was 32. The MAS frequency was 24 kHz.

relaxation delay of this experiment was 15 s. The details of the ^{13}C CP-MAS 2DPASS SSNMR experiment are also discussed in previously published articles.[10−21]

The 2D PASS CP-MAS SSNMR experiment employs a pulse sequence that involves five π pulses with fixed total duration and time intervals determined by PASS-equations, as reported by Antzutkin et al.[49] The ^{13}C nucleus is subjected to a 90° pulse of length 3.3 μs, followed by a relaxation delay of 15 s. Thirteen steps of cogwheel phase cycling COG13 (0, 1, 0, 1, 0, 1, 6) were applied, resulting in a total of 4030 scans (an integral multiple of 13).[60,61] The coherence transfer pathway for this experiment was previously reported by Ghosh et al.[50] In the indirect dimension, acquisition of sixteen data points is required as the number of sidebands is less than sixteen. The CSA tensor was determined using the intensity of the sidebands with the aid of the graphical method.[62] The ^{13}C 2DPASS CP-MAS SSNMR experiments were conducted at two different MAS frequencies, specifically 600 Hz and 2 kHz. The JEOL commercial MAS controller was utilized to stabilize the MAS frequency at (600 ± 4) and (2000 ± 4) Hz. The principal components of CSA parameters are determined by utilizing HBA (http://anorganik.uni-tuebingen.de/klaus/soft/index.php?p=hba/hba) and RMN (https://www.physyapps.com/rmn-intuitive-signal-processing-physical-sciences) software.

CSA interaction provides valuable insights into the molecular structure and dynamics. In static powder samples, CSA can be directly measured by recording powder patterns. However, these experiments suffer from limitations such as poor sensitivity and spectral overlap. To address these challenges, various methods have been developed.[40−49] Most of these recoupling methods rely on analyzing spinning-sideband or powder patterns to extract the CSA parameters. The 2DPASS experiments are not well-suited for CSA measurements in strongly coupled systems since they are unable to efficiently suppress homonuclear dipolar interactions. In our case, we are specifically measuring CSA parameters of ^{13}C carbon nuclei with natural abundance, hence the

https://doi.org/10.1021/acsomega.3c03406
ACS Omega 2023, 8, 24093−24105

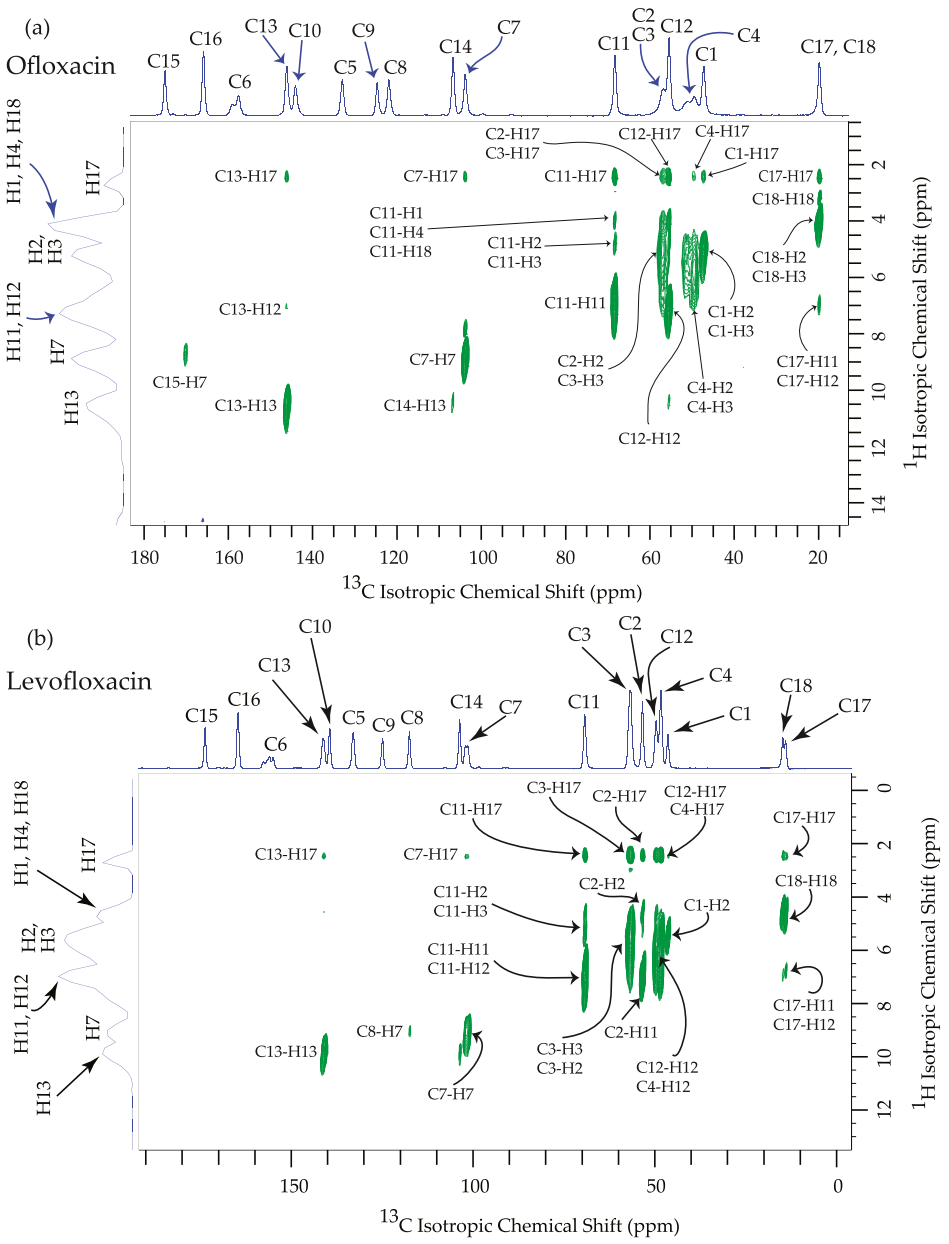

Figure 4. Two-dimensional $^{1}H-^{13}C$ HETCOR SSNMR spectra of (a) ofloxacin and (b) levofloxacin. The experiments were performed using a 600 MHz Bruker Avance Neo spectrometer with a contact time of 200 μs and a recycle delay of 15 s, and the number of scans was 64. The MAS frequency was 10 kHz.

homonuclear dipole−dipole interaction has no role in the observed spinning sideband pattern. However, heteronuclear dipole−dipole interactions, specifically the $^{1}H-^{13}C$ heteronuclear dipolar coupling, need to be decoupled. This can be achieved by utilizing the SPINAL 64 decoupling sequence.

The 2DPASS sequence is employed for CSA parameter measurements, but it is important to note some potential sources of error. One such source is the unoptimized heteronuclear decoupling sequence during t2 evolution, which can introduce inaccuracies. Additionally, the unstable spinning frequency can also impact the reliability of 2DPASS experiments. Lastly, fluctuations in temperature can also affect the measurement of CSA parameters using the 2DPASS experiment.

3. RESULTS AND DISCUSSION

3.1. ^{13}C CP-MAS SSNMR Spectrum of Ofloxacin and Levofloxacin. Figure 2 portrays the ^{13}C CP-MAS SSNMR spectrum of ofloxacin and levofloxacin, wherein the resonance lines are assigned by following the article published by Al-Omar.[59] The intensity of ^{13}C CP-MAS resonance lines associated with different carbon nuclei in a compound is influenced by several factors. The variation in the number of protons surrounding each carbon nucleus and different line widths influence the intensity of ^{13}C CP-MAS resonance lines. Additionally, the mobility of these carbon nuclei, as reflected by their spin−lattice relaxation time, further contributes to the differences observed in resonance line intensity. The mobility of carbon nuclei is particularly significant in the context of cross-polarization efficiency as it affects the strength of the $^{1}H-^{13}C$ heteronuclear dipolar coupling.

https://doi.org/10.1021/acsomega.3c03406
ACS Omega 2023, 8, 24093−24105

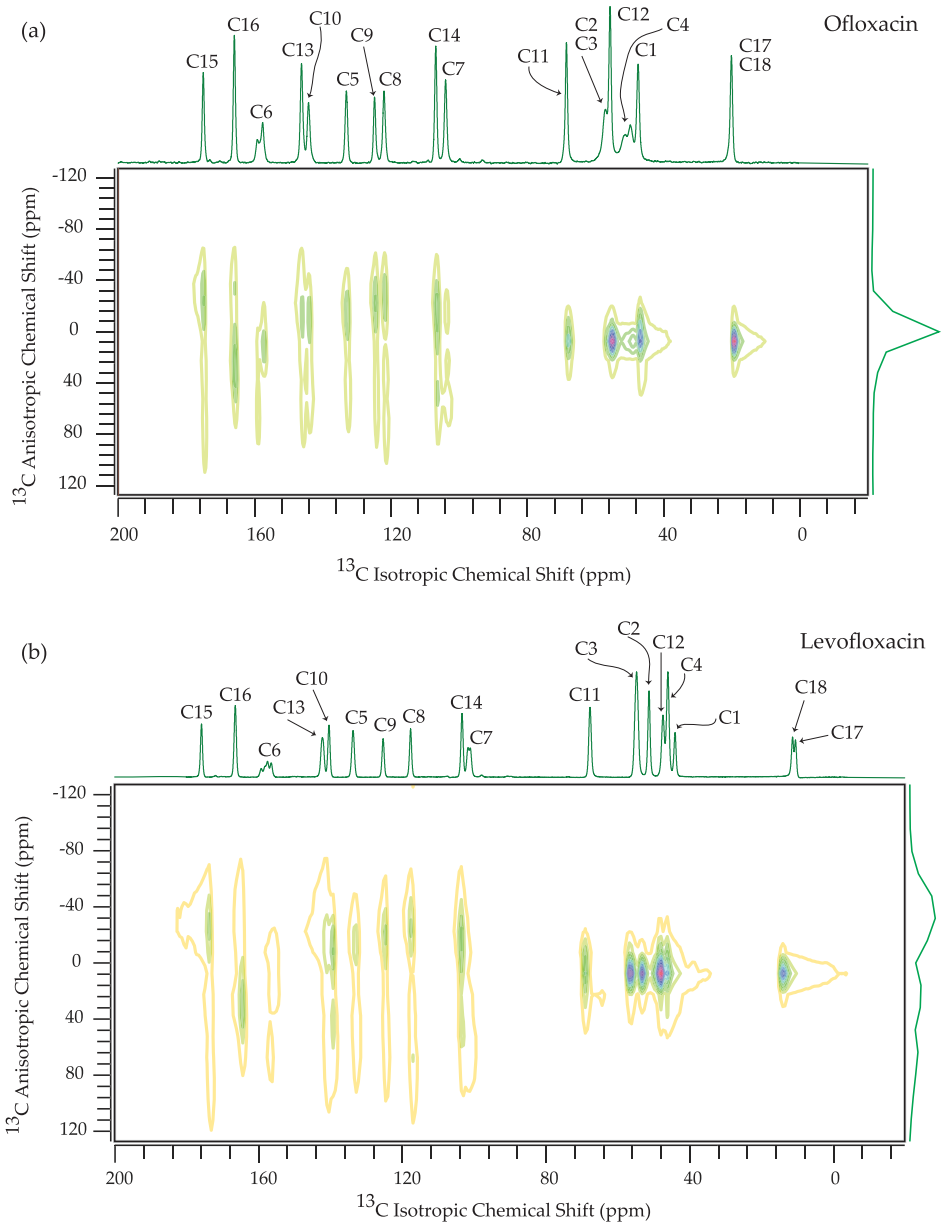

Figure 5. 2DPASS CP-MAS SSNMR spectrum of (a) ofloxacin and (b) levofloxacin. The experiments were performed using a 500 MHz JEOL spectrometer with a contact time of 2 ms and a recycle delay of 15 s, and the number of scans was 4030 (an integral multiple of 13 as 13-step cogwheel-phase cycling was used to perform the 2DPASS experiment). The MAS frequencies were 2 kHz and 600 Hz.

The isotropic as well as anisotropic chemical shift (which will be discussed in the next section) is observed to be the highest for carbonyl group carbons C15 and C16 due to the presence of polar bonds and the magnetic shielding/deshielding effect. The lack of symmetry in the carbonyl group leads to large anisotropic chemical shifts which are manifested due to the presence of three distinct magnetic susceptibilities along the three directions of the principal axis system (PAS). This is also the origin of the two anisotropic susceptibilities, one being parallel and the other being perpendicular to the magnetic field. Another contributing factor to the large value of the chemical shift is the induced polarization of the electron charge distribution surrounding C15 and C16 nuclei owing to the polar bond. The strength of the secondary magnetic field is modified depending on the direction of the induced polarization. The isotropic-chemical shift of C6 nuclei is also found to be large owing to its bonding with the electro-negative fluorine atom. The electron cloud surrounding the C6 carbon nuclei is attracted by the electro-negative atom, which leads to deshielding. The resonance line of C6 nuclei splits owing to the *J*-coupling. The isotropic chemical shift is observed to be the lowest for carbon nuclei residing on the piperazine ring, oxazine ring, and methyl group carbon. Conversely, isotropic chemical shifts are found to be substantially large for carbon nuclei residing on the quinolone ring. Typically, carbon nuclei situated on the aromatic ring exhibit significant isotropic and anisotropic chemical shifts due to the magnetic shielding and deshielding effects stemming from the ring current. As the π electrons of the aromatic ring orbit around the nucleus in a clockwise direction, a secondary magnetic field is generated along the external magnetic field's direction, while the rotation of the π electrons in the counter-clockwise direction causes the secondary magnetic field to be induced in the opposite direction of the external magnetic

https://doi.org/10.1021/acsomega.3c03406
ACS Omega 2023, 8, 24093−24105

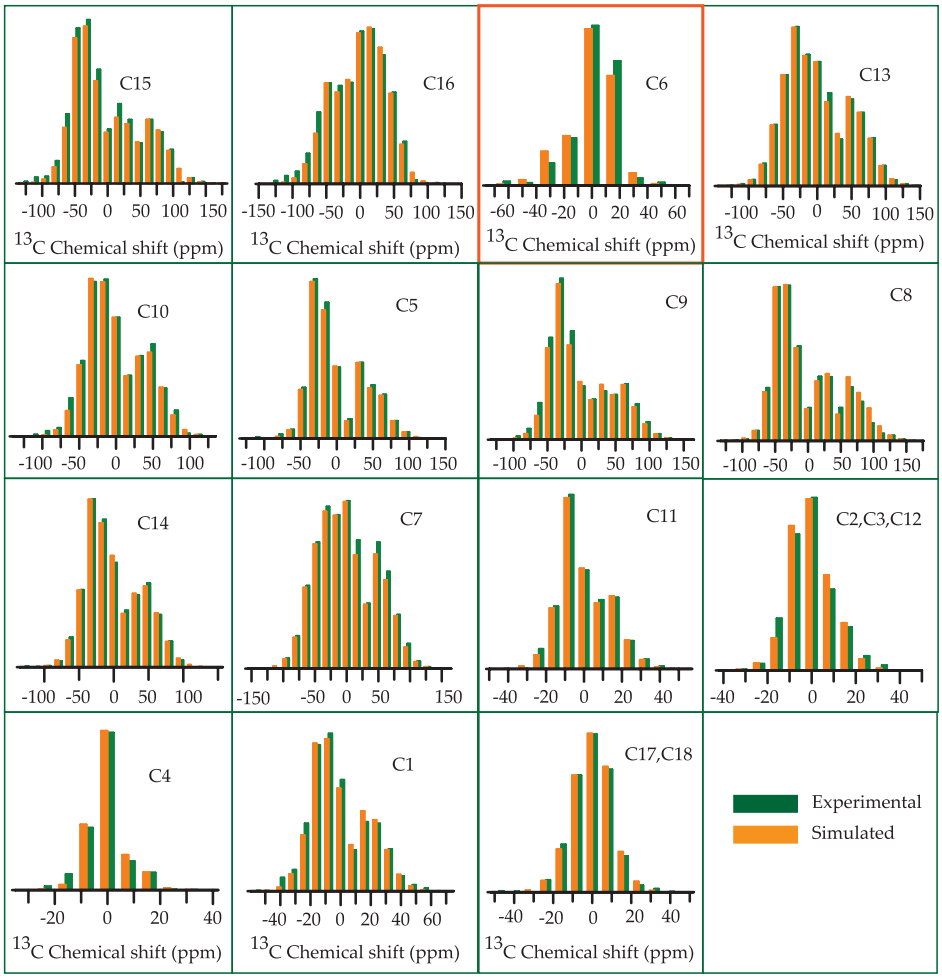

Figure 6. Spinning CSA sideband pattern of crystallographically different carbon nuclei sites of ofloxacin. The span ($\Omega = \delta_{11} - \delta_{33}$) of the CSA pattern of C6 nuclei (the C6 atom is attached with the fluorine atom) is small due to negative hyperconjugation.

field. The effects of these local magnetic fields are known as magnetic shielding and deshielding effects, respectively.

Figure 3 shows the ^{19}F MAS NMR spectrum of both ofloxacin and levofloxacin. Interestingly, despite having only one fluorine atom, levofloxacin displayed two distinct peaks in the ^{19}F spectrum of hemihydrates, as previously noted by Gorman et al.[65] Levofloxacin, being the levo-isomer of ofloxacin, has the ability to crystallize into two different hydrate forms: the monohydrate and the hemihydrate. The ^{19}F MAS SSNMR spectrum reveals that the hemihydrate form of levofloxacin was utilized for the experiments. The presence of two distinct resonance lines in the spectrum can be attributed to the existence of two distinct molecular conformations within the crystal structure, which arises from the occurrence of two molecules in the asymmetric unit cell, as previously observed by Gorman et al.[65] Although ofloxacin has only one fluorine atom, the presence of polymorphism leads to the appearance of small resonance lines alongside the main resonance line in the ^{19}F MAS spectrum (as shown in Figure 3a).[66,67]

3.2. ^{13}C−^{1}H FSLGHETCOR Spectrum of Ofloxacin and Levofloxacin. The molecular motional dynamics strongly impact the ^{1}H−^{13}C heteronuclear dipolar coupling, which can be examined using the 2D ^{1}H−^{13}C proton-detected FSLGHETCOR spectrum, as depicted in Figure 4. The assignment of ^{1}H and ^{13}C resonance lines is done by following the article by Al-Omar.[59] A relatively strong ^{1}H−^{13}C dipolar coupling indicates slower molecular dynamics. In ofloxacin, heteronuclear correlations between C15 and H7 nuclei and C13 and H12 nuclei are observable (as depicted in Figure 4), yet these are absent in levofloxacin. The close spatial proximity between C4 and H12, and between C4 and H17, suggests the proximate location of the piperazine and oxazine rings.

3.3. Determination of Principal Components of CSA Parameters of Ofloxacin and Levofloxacin. The present study showcases Figure 5, which exhibits the 2DPASS CP-MAS SSNMR spectrum of (a) ofloxacin and (b) levofloxacin. This spectrum demonstrates the correlation between the isotropic and anisotropic chemical shifts of the two enantiomers. The direct dimension portrays the purely isotropic spectrum, also known as the "infinite spinning frequency spectrum", whereas the indirect dimension represents the anisotropic spectrum. The CSA measurements on ofloxacin and levofloxacin, presented in Figures 6 and 7, display the "negative hyperconjugation" effect for C6 nuclei sites. Both of these fluoroquinolones possess fluorine attached to their C6 carbon nuclei. The CSA sideband pattern of C6 nuclei, as shown in Table 1, displays substantially lower "span" and "anisotropy" values than other carbon nuclei residing on the quinolone ring. In the phenomenon known as "negative hyperconjugation", the electron density is transferred from carbon−carbon (C−C) or carbon−hydrogen (C−H) σ orbitals to the carbon−fluorine (C−F) antibonding σ^* orbital.

https://doi.org/10.1021/acsomega.3c03406
ACS Omega 2023, 8, 24093−24105

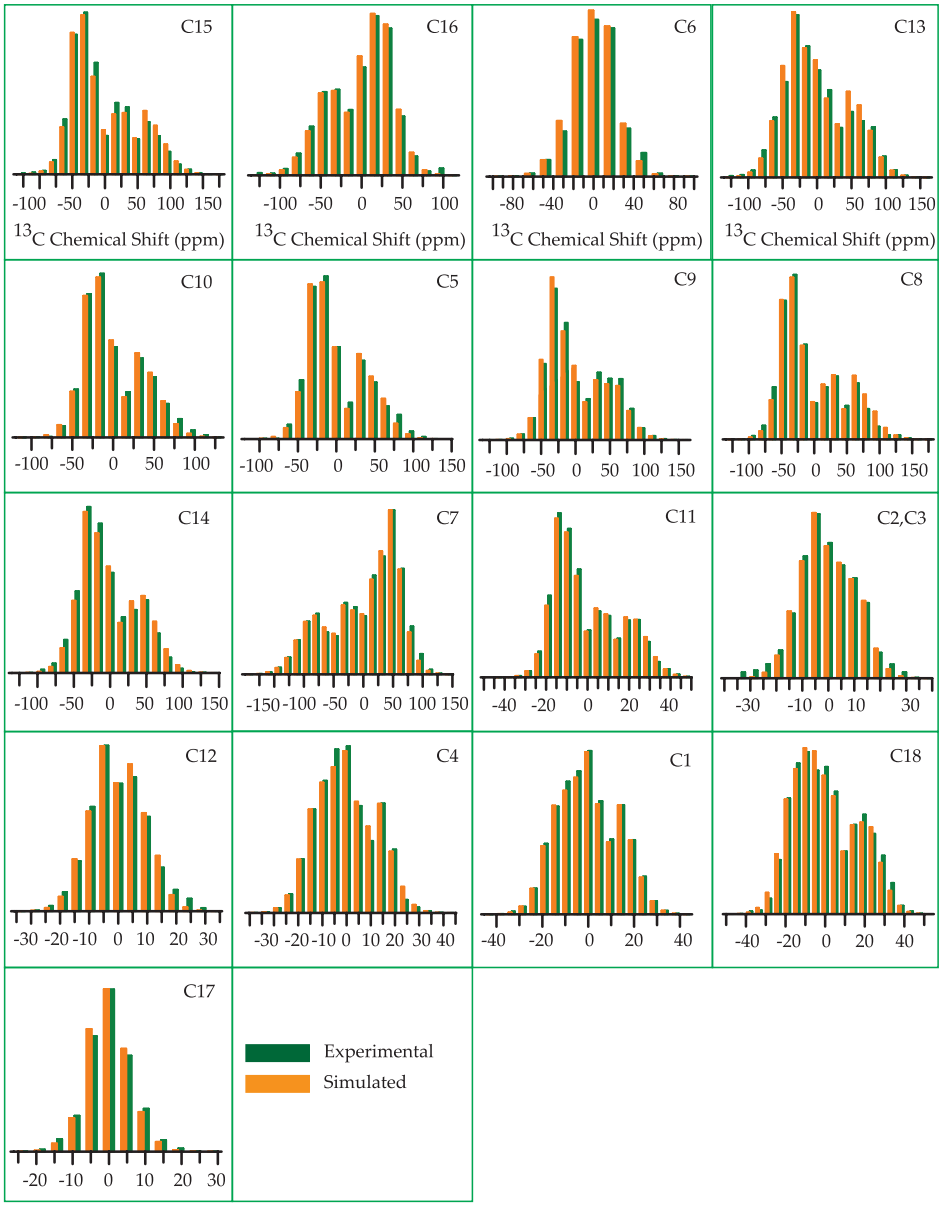

Figure 7. Spinning CSA sideband pattern of crystallographically different carbon nuclei sites of levofloxacin. The span ($\Omega = \delta_{11} - \delta_{33}$) of the CSA pattern of C6 nuclei (the C6 atom is attached with the fluorine atom) is small due to negative hyperconjugation.

This transfer occurs because the C−F antibonding orbital acts as an electron acceptor, while the C−C or C−H bonding orbital acts as an electron donor. As a result of this electron transfer, the electron density surrounding C6 is localized, which accounts for the nuclear shielding effect. This localization of electron density leads to a reduction in the effective magnetic field experienced by C6 nuclei, resulting in lower values of the principal components of CSA parameters. The presence of a fluorine atom at the C6 position enhances the gyrase inhibition and cell penetration abilities of quinolones, making them effective against microorganisms that are resistant to other antibacterial agents.[1−5] The spinning CSA sideband pattern on C6 nuclei of ofloxacin is nearly axially symmetric, while it is highly asymmetric for levofloxacin, indicating the dissimilarity in the electronic distribution surrounding C6 nuclei in ofloxacin and levofloxacin.

The spinning CSA sideband pattern furnishes critical insights into the electron density distribution enveloping the nucleus, molecular motion, and the orientation of the molecule in relation to the local magnetic field. A substantial disparity in the "span ($\Omega = \delta_{11} - \delta_{33}$)" of the spinning CSA sideband pattern was observed for C15, C10, and C7 nuclei between ofloxacin and levofloxacin. While the spinning CSA sideband pattern of C4 nuclei was axially symmetric (with the anisotropy parameter $\eta = (\delta_{22} - \delta_{11})/(\delta_{33} - \delta_{iso})$ being zero) for ofloxacin, it exhibited a high degree of asymmetry for the same nuclei in levofloxacin. A remarkable difference in the anisotropy parameter ($\Delta\delta = \delta_{33} - (\delta_{11} + \delta_{22})/2$) of C7 nuclei was also noted between ofloxacin and levofloxacin. Ofloxacin has an anisotropy parameter of 139.9 ppm, while levofloxacin has −200.4 ppm, signifying that the maximum separation distance lies on the opposite sides of the center of gravity of C7 nuclei for these enantiomers. It is also worth mentioning that the value of δ_{22} of C15 is shifted toward the higher frequency side in ofloxacin compared to that in levofloxacin. The δ_{22} value of the keto group carbon reflects the hydrogen bonding

https://doi.org/10.1021/acsomega.3c03406
ACS Omega 2023, 8, 24093−24105

Table 1. Values of the Principal Components of CSA Parameters of Ofloxacin and Levofloxacin[a]

antibiotics	carbon nuclei	isotropic chemical shift (δ_{iso}) (ppm)	δ_{11} (ppm)	δ_{22} (ppm)	δ_{33} (ppm)	span (ppm)	anisotropy (ppm) $\Delta\delta = \delta_{33} - \frac{(\delta_{11} + \delta_{22})}{2}$	asymmetry	skew $\hat{k} = \frac{3\delta_{22} - \delta_{iso}}{\delta_{11} - \delta_{33}}$
ofloxacin	C15	176.0	290.2 ± 1.4	137.5 ± 1.2	99.4 ± 0.8	191.0 ± 1.2	171.7 ± 2.2	0.3	−0.6
levofloxacin	C15	174.0	284.5 ± 0.7	127.0 ± 0.6	109.5 ± 0.4	175.0 ± 0.7	166.2 ± 1.1	0.1	−0.8
ofloxacin	C16	166.4	233.2 ± 2.3	176.0 ± 1.7	90.1 ± 1.5	143.1 ± 2.4	−114.5 ± 2.2	0.7	0.2
levofloxacin	C16	165.0	227.0 ± 0.6	184.0 ± 0.5	84.0 ± 0.4	143.1 ± 0.6	−122.0 ± 0.6	0.5	0.4
ofloxacin	C6	158.0	182.4 ± 0.7	173.0 ± 0.5	119.0 ± 0.5	63.6 ± 1.0	−59.0 ± 0.8	0.2	0.7
levofloxacin	C6	156.1	194.5 ± 1.0	159.0 ± 0.6	115.0 ± 0.8	79.5 ± 1.6	−61.6 ± 1.2	0.9	0.1
ofloxacin	C13	146.0	245.1 ± 1.5	122.7 ± 1.2	70.2 ± 0.9	175.0 ± 1.3	148.7 ± 2.3	0.5	−0.4
levofloxacin	C13	141.5	240.6 ± 1.5	118.2 ± 1.2	65.7 ± 0.9	175.0 ± 1.4	148.7 ± 2.3	0.5	−0.4
ofloxacin	C10	144.6	225.7 ± 1.1	125.5 ± 0.9	82.5 ± 0.8	143.1 ± 1.2	121.6 ± 1.7	0.5	−0.4
levofloxacin	C10	140.0	221.0 ± 0.5	119.1 ± 0.3	94.0 ± 0.3	127.2 ± 0.6	114.5 ± 0.7	0.3	−0.6
ofloxacin	C5	133.5	218.3 ± 1.5	91.1 ± 1.1	91.1 ± 0.9	127.2 ± 1.5	127.2 ± 2.3	0.0	−1.0
levofloxacin	C5	133.1	211.6 ± 0.8	103.4 ± 0.6	84.3 ± 0.5	127.2 ± 0.9	118.0 ± 1.2	0.2	−0.7
ofloxacin	C9	124.4	225.1 ± 1.0	82.0 ± 0.8	66.1 ± 0.6	159.0 ± 0.8	151.0 ± 1.5	0.1	−0.8
levofloxacin	C9	125.0	220.2 ± 0.9	92.9 ± 0.7	61.1 ± 0.5	159.0 ± 0.8	143.1 ± 1.4	0.3	−0.6
ofloxacin	C8	122.0	236.0 ± 1.0	69.5 ± 0.8	60.8 ± 0.6	175.0 ± 0.9	170.5 ± 1.5	0.1	−0.9
levofloxacin	C8	117.6	231.3 ± 1.6	65.1 ± 1.3	56.3 ± 0.9	175.0 ± 1.2	170.6 ± 2.4	0.1	−0.9
ofloxacin	C14	106.2	192.3 ± 0.3	82.7 ± 0.2	43.6 ± 0.2	146.7 ± 0.3	129.1 ± 1.2	0.4	−0.5
levofloxacin	C14	104.0	187.4 ± 0.8	80.0 ± 0.6	44.2 ± 0.5	143.2 ± 0.9	125.3 ± 1.2	0.4	−0.5
ofloxacin	C7	103.3	196.6 ± 1.2	91.6 ± 1.2	21.7 ± 1.2	175.0 ± 1.1	140.0 ± 1.2	0.7	−0.2
levofloxacin	C7	102.1	191.2 ± 1.3	146.6 ± 4.1	−31.5 ± 2.7	223.0 ± 3.4	−200.4 ± 4.0	0.3	0.6
ofloxacin	C11	69.0	96.5 ± 0.7	60.7 ± 0.5	48.8 ± 0.5	47.7 ± 0.9	41.7 ± 1.1	0.4	−0.5
levofloxacin	C11	69.4	104.7 ± 0.2	56.0 ± 0.1	47.4 ± 0.1	57.3 ± 0.2	53.0 ± 0.3	0.2	−0.7
ofloxacin	C2, C3	56.0	77.2 ± 0.3	53.3 ± 0.2	37.4 ± 0.2	40.0 ± 0.4	31.8 ± 0.4	0.7	−0.2
levofloxacin	C3	57.0	76.4 ± 0.4	55.4 ± 0.3	38.2 ± 0.3	38.2 ± 0.5	29.6 ± 0.6	0.9	−0.1
levofloxacin	C2	53.7	70.4 ± 0.4	53.7 ± 0.3	36.9 ± 0.3	33.4 ± 0.5	−25.0 ± 0.4	1.0	0.0
ofloxacin	C12	56.0	77.2 ± 0.3	53.3 ± 0.2	37.4 ± 0.2	39.7 ± 0.4	32.0 ± 0.4	0.7	−0.2
levofloxacin	C12	50.0	74.5 ± 0.7	48.3 ± 0.6	27.0 ± 0.5	48.0 ± 0.7	37.0 ± 1.1	0.9	−0.1
ofloxacin	C4	49.6	65.5 ± 0.1	41.6 ± 0.08	41.6 ± 0.09	24.0 ± 0.1	24.0 ± 0.2	0.0	−1.0
levofloxacin	C4	48.4	76.4 ± 0.7	45.0 ± 0.6	24.0 ± 0.4	52.5 ± 0.6	42.0 ± 1.0	0.7	−0.2
ofloxacin	C1	47.6	89.3 ± 0.7	35.6 ± 0.5	18.0 ± 0.4	71.5 ± 0.7	62.6 ± 1.0	0.9	−0.5
levofloxacin	C1	46.4	80.5 ± 0.5	40.2 ± 0.4	18.5 ± 0.3	62.0 ± 0.4	51.2 ± 0.8	0.6	−0.3
levofloxacin	C18	15.1	27.4 ± 0.1	14.3 ± 0.1	3.5 ± 0.1	23.8 ± 0.1	18.5 ± 0.2	0.9	−0.1
ofloxacin	C17C18	20.0	40.0 ± 0.1	20.0 ± 0.1	0.1 ± 0.09	40.0 ± 0.1	−30.0 ± 0.1	1.0	0.0
levofloxacin	C17	14.5	27.0 ± 0.1	14.0 ± 0.1	3.0 ± 0.1	24.0 ± 0.1	18.5 ± 0.2	0.9	−0.1

[a]The magnitude of the anisotropy parameter $\Delta\delta = \delta_{33} - (\delta_{11} + \delta_{22})/2$ determines the largest distance of separation of the spinning CSA sideband pattern from the center of gravity ($\delta_{iso} = (\delta_{11} + \delta_{22} + \delta_{33})/3$), and the sign of the anisotropy parameter indicates the side of the center of gravity where the separation distance is maximal. The asymmetry parameter $\eta = (\delta_{22} - \delta_{11})/(\delta_{33} - \delta_{iso})$ measures how much the spinning CSA sideband pattern is deviated from its axially symmetric value. Skew $\hat{k} = (3\delta_{22} - \delta_{iso})/(\delta_{11} - \delta_{33})$ measures the orientation of the asymmetry of the spinning CSA sideband pattern.

https://doi.org/10.1021/acsomega.3c03406
ACS Omega 2023, 8, 24093−24105

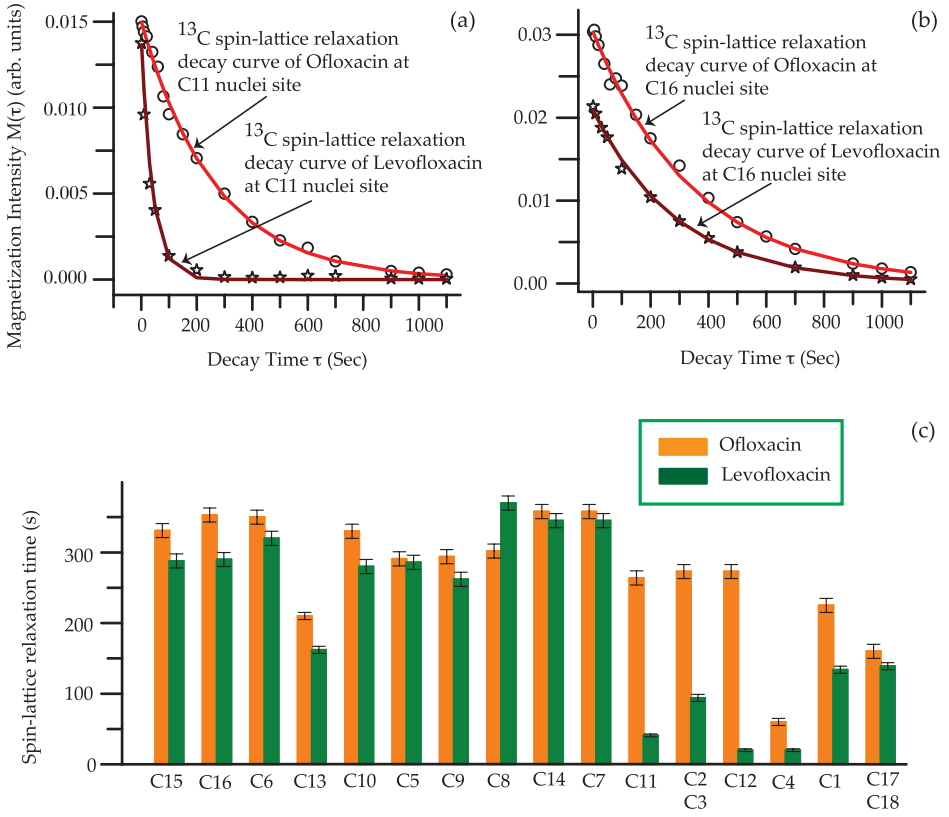

Figure 8. ^{13}C magnetization decay curve of ofloxacin and levofloxacin at (a) C11 and (b) C16 carbon nuclei sites. (c) It is clear from the bar diagram that except at C8 carbon nuclei sites, the spin−lattice relaxation rate is increased in levofloxacin compared to that in ofloxacin. The experiments were performed using a 500 MHz JEOL spectrometer with a contact time of 2 ms and a recycle delay of 15 s, and the number of scans was 2048. The MAS frequency was 10 kHz.

strength associated with the group, which decreases when it shifts toward the higher frequency side.[63,64]

3.4. Determination of the Site-Specific Spin−Lattice Relaxation Time of Ofloxacin and Levofloxacin. The ^{13}C spin−lattice relaxation time, as depicted in Figure 8 and Table 2, reveals that the motional dynamics is larger for all the nuclei sites of levofloxacin, except for C8, in comparison to that of ofloxacin. Notably, the spin−lattice relaxation time of carbon nuclei residing on the piperazine and oxazine rings of levofloxacin is significantly reduced compared to that of ofloxacin, which may account for the higher bioavailability of levofloxacin. This phenomenon is reminiscent of the correlation between the potency of steroids and the spin−lattice relaxation time, as previously established by SSNMR measurements on glucocorticoids.[21] The glucocorticoids with increased potency due to the substitution of various functional groups exhibited shorter spin−lattice relaxation times, indicating that there may exist a correlation between the potency of the drug and nuclear spin dynamics.[21]

Several studies have reported that the antibacterial activity of levofloxacin is significantly higher than that of ofloxacin.[5] In this study, we measured the spin−lattice relaxation time at each crystallographically distinct carbon nuclei site of both ofloxacin and levofloxacin and found that the spin−lattice relaxation time is shorter in ofloxacin compared to that in levofloxacin, except for the C8 nuclei. The spin−lattice relaxation time is highly correlated with the motional dynamics of the molecule, and it has been shown by the SSNMR measurement that molecular degrees of freedom are strongly linked to solubility[50,53,55] as well as bioavailability.[21]

Table 2. Spin−Lattice Relaxation Time and Local Correlation Time of Ofloxacin and Levofloxacin at Crystallographically Different Carbon Sites

ofloxacin		levofloxacin	
carbon nuclei	spin−lattice relaxation time (s)	carbon nuclei	spin−lattice relaxation time (s)
C15	331 ± 10	C15	288 ± 10
C16	353 ± 10	C16	290 ± 10
C6	350 ± 10	C6	320 ± 10
C13	210 ± 5	C13	162 ± 5
C10	330 ± 10	C10	280 ± 10
C5	291 ± 10	C5	286 ± 10
C9	294 ± 10	C9	262 ± 10
C8	302 ± 10	C8	370 ± 10
C14	358 ± 10	C14	345 ± 10
C7	358 ± 10	C7	345 ± 10
C11	264 ± 10	C11	41 ± 3
C2,C3	273 ± 10	C2,C3	94 ± 5
C12	273 ± 10	C12	20 ± 2
C4	60 ± 5	C4	26 ± 2
C1	225 ± 10	C1	134 ± 5
C17, C18	160 ± 10	C18	131 ± 5
		C17	139 ± 5

Moreover, bioavailability is also closely tied to the bioactivity of the drug molecule. Therefore, it is reasonable to suggest that there may be a correlation between the nuclear spin−lattice relaxation time and the bioactivity of the drug and that the gradual decrement of the spin−lattice relaxation time of

https://doi.org/10.1021/acsomega.3c03406
ACS Omega 2023, 8, 24093−24105

levofloxacin compared to that of ofloxacin may be one of the molecular origins of the higher antibacterial activity of levofloxacin. These findings have important implications for the design and development of new antibiotics with improved efficacy.

4. CONCLUSIONS

The NMR relaxometry revealed that the spin−lattice relaxation time is shorter in ofloxacin compared to that in levofloxacin, except for the C8 nuclei. The spin−lattice relaxation time, which is strongly linked to molecular motion, has been shown to be highly correlated with solubility and bioavailability.[21,50,53,55] Furthermore, bioavailability is closely associated with the bioactivity of the drug molecule. Based on these findings, it is reasonable to suggest that there may be a correlation between nuclear spin−lattice relaxation time and the bioactivity of the drug and that the gradual decrement of the spin−lattice relaxation time of levofloxacin compared to that of ofloxacin may be one of the molecular origins of the higher antibacterial activity of levofloxacin.

The variations in the CSA parameters for certain carbon nuclei sites like C4, C7, C10, and C15 suggest that the local electronic environment surrounding certain nuclei of the two enantiomers is different. The heteronuclear correlation between C15 and H7 nuclei and C13 and H12 nuclei is observed in ofloxacin, but the $^{1}H-^{13}C$ correlation among those nuclei is absent in levofloxacin.

These types of variations in the local electronic configuration and the nuclear spin dynamics between the two enantiomers have been thoroughly studied for the first time by applying SSNMR methodologies. The correlation between the bioavailability and nuclear spin dynamics can also be established by NMR relaxometry. Such an in-depth analysis of the structure and dynamics of antibiotics at the atomic-scale resolution using NMR crystallographic approaches will prove beneficial for advanced drug design.

■ ASSOCIATED CONTENT

Supporting Information

The Supporting Information is available free of charge at https://pubs.acs.org/doi/10.1021/acsomega.3c03406.

Single-crystal XRD analysis of ofloxacin and levofloxacin; comparison of lattice energy and conformation; and energy framework representation of levofloxacin and ofloxacin (PDF)

■ AUTHOR INFORMATION

Corresponding Authors

Krishna Kishor Dey − *Department of Physics, Dr. Harisingh Gour Central University, Sagar 470003 Madhya-Pradesh, India*; Email: dey.krishna@gmail.com

Manasi Ghosh − *Physics Section, Mahila Maha Vidyalaya, Banaras Hindu University, Varanasi 221005 Uttar-Pradesh, India*; orcid.org/0000-0002-8472-0288; Email: manasi.ghosh@bhu.ac.in

Authors

Bijay Laxmi Pradhan − *Department of Physics, Institute of Science, Banaras Hindu University, Varanasi 221005 Uttar-Pradesh, India; Physics Section, Mahila Maha Vidyalaya, Banaras Hindu University, Varanasi 221005 Uttar-Pradesh, India*

Jai Prakash Yadav − *Physics Section, Mahila Maha Vidyalaya, Banaras Hindu University, Varanasi 221005 Uttar-Pradesh, India*

Lekhan Lodhi − *Department of Zoology, Dr. Harisingh Gour Central University, Sagar 470003 Madhya-Pradesh, India*

Prince Sen − *Department of Physics, Dr. Harisingh Gour Central University, Sagar 470003 Madhya-Pradesh, India*

Complete contact information is available at: https://pubs.acs.org/10.1021/acsomega.3c03406

Notes

The authors declare no competing financial interest.

■ ACKNOWLEDGMENTS

The author Manasi Ghosh is grateful to Science and Engineering Research Board (SERB)-POWER research grant (file no. SPG/2021/000303), Department of Science and Technology (DST), Government of India, IoE-BHU Seed Grant-II (Dev. Scheme no. 6031(B)), for financial support. The authors are thankful to DST sponsored SATHI-BHU scheme no. 6025 for providing a 600 MHz SSNMR facility and to Dr. Harisingh Gour University for providing a 500 MHz SSNMR facility.

■ REFERENCES

(1) Hooper, D. C. Mechanisms of fluoroquinolone resistance. *Drug Resistance Updates* **1999**, *2*, 38−55.

(2) Zechiedrich, E. L.; Cozzarelli, N. R. Roles of topoisomerase IV and DNA gyrase in DNA unlinking during replication in Escherichia coli. *Genes Dev.* **1995**, *9*, 2859−2869.

(3) Davis, R.; Bryson, H. M. Levofloxacin. *Drugs* **1994**, *47*, 677−700.

(4) Liu, X.; Liu, Y.; Lu, S.; Wang, Z.; Wang, Y.; Zhang, G.; Guo, X.; Guo, W.; Zhang, T.; Xi, B. Degradation difference of ofloxacin and levofloxacin by UV/H_2O_2 and UV/PS (persulfate): Efficiency, factors and mechanism. *Chem. Eng. J.* **2020**, *385*, 123987.

(5) North, D. S.; Fish, D. N.; Redington, J. J. Levofloxacin, a second-generation fluoroquinolone. *Pharmacotherapy* **1998**, *18*, 915−935.

(6) Freitas, J. T. J.; de Melo, C. C.; Viana, O. M. M. S.; Ferreira, F. F.; Doriguetto, A. C. Crystal Structure of Levofloxacin Anhydrates: A High-Temperature Powder X-ray Diffraction Study Versus Crystal Structure Prediction. *Cryst. Growth Des.* **2018**, *18*, 3558−3568.

(7) Hoshino, K.; Sato, K.; Akahane, K.; Yoshida, A.; Hayakawa, I.; Sato, M.; Une, T.; Osada, Y. Significance of the methyl group on the oxazine ring of ofloxacin derivatives in the inhibition of bacterial and mammalian type II topoisomerases. *Antimicrob. Agents Chemother.* **1991**, *35*, 309−312.

(8) Mu, H.; Lei, H.; Wang, B.; Xu, Z.; Zhang, C.; Ling, L.; Tian, Y.; Hu, J.; Sun, Y. Molecular Modeling Application on Hapten Epitope Prediction: An Enantioselective Immunoassay for Ofloxacin Optical Isomers. *J. Agric. Food Chem.* **2014**, *62*, 7804−7812.

(9) He, L.; Liang, Z.; Yu, G.; Li, X.; Chen, X.; Zhou, Z.; Ren, Z. Green and Efficient Resolution of Racemic Ofloxacin Using Tartaric Acid Derivatives via Forming Cocrystal in Aqueous Solution. *Cryst. Growth Des.* **2018**, *18*, 5008−5020.

(10) Dey, K. K.; Deshmukh, M.; Ghosh, M. A Description of the Local Structure and Dynamics of Ketoconazole Molecule by Solid-State NMR Measurements and DFT Calculations: Proposition for NMR Crystallography. *ChemistrySelect* **2021**, *6*, 10208−10220.

(11) Dey, K. K.; Lodhi, L.; Ghosh, M. Study of the Variation of the Electronic Distribution and Motional Dynamics of Two Independent Molecules of an Asymmetric Unit of Atorvastatin Calcium by Solid-State NMR Measurements. *ACS Omega* **2021**, *6*, 22752−22764.

(12) Dey, K. K.; Ghosh, M. Study of the Structure and Dynamics at Various Parts of the Antibacterial Drug Molecule Cefpodoxime proxetil. *Solid State Nucl. Magn. Reson.* **2021**, *115*, 101752.

(13) Dey, K. K.; Ghosh, M. Investigation of the Structure and Dynamics of Antiviral Drug Adefovir Dipivoxil by Site-Specific Spin−Lattice Relaxation Time Measurements and Chemical Shift Anisotropy Tensor Measurements. *ACS Omega* **2020**, *5*, 29373−29381.
(14) Dey, K. K.; Ghosh, M. Determination of Chemical Shift Anisotropy Tensor and Molecular Correlation Time of Proton Pump Inhibitor Omeprazole by Solid State NMR Measurements. *New J. Chem.* **2020**, *44*, 19393−19403.
(15) Dey, K. K.; Ghosh, M. Determination of the Correlation between the Structure and Dynamics of Deflazacort by solid state NMR measurements. *New J. Chem.* **2020**, *44*, 18419−18430.
(16) Dey, K. K.; Ghosh, M. Understanding the Structure and Dynamics of Anti-inflammatory Corticosteroid Dexamethasone by solid state NMR Spectroscopy. *RSC Adv.* **2020**, *10*, 37564−37575.
(17) Dey, K. K.; Gayen, S.; Ghosh, M. Understanding the correlation between structure and dynamics of clocortolone pivalate by solid state NMR measurement. *RSC Adv.* **2020**, *10*, 4310−4321.
(18) Ghosh, M.; Gayen, S.; Dey, K. K. An atomic resolution description of folic acid using solid state NMR measurements. *RSC Adv.* **2020**, *10*, 24973−24984.
(19) Dey, K. K.; Gayen, S.; Ghosh, M. Investigation of the Detailed Internal Structure and Dynamics of Itraconazole by Solid-State NMR Measurements. *ACS Omega* **2019**, *4*, 21627−21635.
(20) Lodhi, L.; Yadav, J. P.; Yamazaki, T.; Duong, N. T.; Poojary, S. L.; Dey, K. K.; Nishiyama, Y.; Ghosh, M. NMR Crystallographic Approach to Study the Variation of the Dynamics of Quinine and Its Quasienantiomer Quinidine. *J. Phys. Chem. C* **2022**, *126*, 17291−17305.
(21) Yadav, J. P.; Lodhi, L.; Fatma, T.; Dey, K. K.; Ghosh, M. Investigation of the Influence of Various Functional Groups on the Dynamics of Glucocorticoids. *ACS Omega* **2022**, *7*, 43190−43209.
(22) Nishiyama, Y.; Hou, G.; Agarwal, V.; Su, Y.; Ramamoorthy, A. Ultrafast Magic Angle Spinning Solid-State NMR Spectroscopy: Advances in Methodology and Applications. *Chem. Rev.* **2023**, *123*, 918−988.
(23) Zhang, R.; Chen, Y.; Rodriguez-Hornedo, N.; Ramamoorthy, A. Enhancing NMR Sensitivity of Natural-Abundance Low-γ Nuclei by Ultrafast Magic-Angle-Spinning Solid-State NMR Spectroscopy. *ChemPhysChem* **2016**, *17*, 2962−2966.
(24) Nicholas, M. P.; Eryilmaz, E.; Ferrage, F.; Cowburn, D.; Ghose, R. Nuclear spin relaxation in isotropic and anisotropic media. *Prog. Nucl. Magn. Reson. Spectrosc.* **2010**, *57*, 111−158.
(25) Anet, F. A. L.; O'Leary, D. J. The shielding tensor part II: Understanding its strange effects on relaxation. *Concepts Magn. Reson.* **1992**, *4*, 35−52.
(26) Orendt, A. M.; Facelli, J. C. Solid state effects on NMR chemical shifts. *Annu. Rep. NMR Spectrosc.* **2007**, *62*, 115−178.
(27) Dais, P.; Spyros, A. ^{13}C nuclear magnetic relaxation and local dynamics of synthetic polymers in dilute solution and in the bulk state. *Prog. Nucl. Magn. Reson. Spectrosc.* **1995**, *27*, 555−633.
(28) Wylie, B. J.; Rienstra, C. M. Multidimensional solid state NMR of anisotropic interactions in peptides and proteins. *J. Chem. Phys.* **2008**, *128*, 052207.
(29) Veeman, W. S. Carbon-13 Chemical Shift Anisotropy. *Prog. Nucl. Magn. Reson. Spectrosc.* **1984**, *16*, 193−235.
(30) Shao, L.; Crockford, C.; Geen, H.; Grasso, G.; Titman, J. J. Chemical Shift Anisotropy Amplification. *J. Magn. Reson.* **2004**, *167*, 75−86.
(31) Wu, G. Solid-state ^{17}O NMR studies of organic and biological molecules. *Prog. Nucl. Magn. Reson. Spectrosc.* **2008**, *52*, 118−169.
(32) *Solid State NMR of Polymers*; Ando, I., Asakura, T., Eds.; Elsevier Science: Amsterdam, 1998.
(33) Antzutkin, O. N. *Solid-State NMR Spectroscopy: Principles and Applications*; Duer, M. J., Eds.; Blackwell Sciences: Oxford, 2002; p 280.
(34) *NMR Spectroscopy of Biological Solids*; Ramamoorthy, A., Ed.; CRC Press: Cleveland, 2005.
(35) Sen, S. Dynamics in Inorganic Glass-forming Liquids by NMR Spectroscopy. *Prog. Nucl. Magn. Reson. Spectrosc.* **2020**, *116*, 155−176.
(36) Duer, M. J. *Solid State NMR Spectroscopy Principles and Applications*; Blackwell Science, 2007.
(37) Pople, J. A. The theory of chemical shifts in nuclear magnetic resonance. I. Induced current densities. *Proc. R. Soc. London, Ser. A* **1957**, *239*, 541−549.
(38) Pople, J. A. Nuclear magnetic resonance in diamagnetic materials. The theory of chemical shifts. *Discuss. Faraday Soc.* **1962**, *34*, 7−14.
(39) Saitô, H.; Ando, I.; Ramamoorthy, A. Chemical shift tensor − The heart of NMR: Insights into biological aspects of proteins. *Prog. Nucl. Magn. Reson. Spectrosc.* **2010**, *57*, 181−228.
(40) Tycko, R.; Dabbagh, G.; Mirau, P. A. Determination of chemical shift anisotropy lineshapes in a two-dimensional magic angle spinning NMR experiment. *J. Magn. Reson.* **1989**, *85*, 265−274.
(41) Liu, S. F.; Mao, J. D.; Schmidt-Rohr, K. A robust technique for two-dimensional separation of undistorted chemical shift anisotropy powder patterns in magic angle spinning NMR. *J. Magn. Reson.* **2002**, *155*, 15−28.
(42) Chan, J. C. C.; Tycko, R. Recoupling of chemical shift anisotropies in solid state NMR under high speed magic angle spinning and in uniformly ^{13}C labelled systems. *J. Chem. Phys.* **2003**, *118*, 8378−8389.
(43) Hou, G.; Byeon, I. J. L.; Ahn, J.; Gronenborn, A. M.; Polenova, T. Recoupling of chemical shift anisotropy by R-symmetry sequences in magic angle spinning NMR spectroscopy. *J. Chem. Phys.* **2012**, *137*, 134201−134210.
(44) Bax, A. D.; Szeverenyi, N. M.; Maciel, G. E. Correlation of isotropic shifts and chemical shift anisotropies by two-dimensional Fourier-transform magic angle hopping NMR spectroscopy. *J. Magn. Reson.* **1983**, *52*, 147−152.
(45) Bax, A. D.; Szeverenyi, N. M.; Maciel, G. E. Chemical shift anisotropy in powdered solids studied by 2D FT CP/MAS NMR. *J. Magn. Reson.* **1983**, *51*, 400−408.
(46) Bax, A. D.; Szeverenyi, N. M.; Maciel, G. E. Chemical shift anisotropy in powdered solids studied by 2D FT NMR with flipping of the spinning axis. *J. Magn. Reson.* **1983**, *55*, 494−497.
(47) Gan, Z. High-resolution chemical shift and chemical shift anisotropy correlation in solids using slow magic angle spinning. *J. Am. Chem. Soc.* **1992**, *114*, 8307−8309.
(48) Dixon, W. T. Spinning-sideband-free and spinning-sideband-only NMR spectra in spinning samples. *J. Chem. Phys.* **1982**, *77*, 1800−1809.
(49) Antzutkin, O. N.; Shekar, S. C.; Levitt, M. H. Two-dimensional sideband separation in magic angle spinning NMR. *J. Magn. Reson., Ser. A* **1995**, *115*, 7−19.
(50) Ghosh, M.; Sadhukhan, S.; Dey, K. K. Elucidating the internal structure and dynamics of α-chitin by 2DPASS-MAS-NMR and spin-lattice relaxation measurements. *Solid State Nucl. Magn. Reson.* **2019**, *97*, 7−16.
(51) Ghosh, M.; Prajapati, B. P.; Kango, N.; Dey, K. K. A comprehensive and comparative study of the internal structure and dynamics of natural β-keratin and regenerated β-keratin by solid state NMR spectroscopy. *Solid State Nucl. Magn. Reson.* **2019**, *101*, 1−11.
(52) Ghosh, M.; Kango, N.; Dey, K. K. Investigation of the internal structure and dynamics of cellulose by ^{13}C-NMR relaxometry and 2DPASS-MAS-NMR measurements. *J. Biomol. NMR* **2019**, *73*, 601−616.
(53) Dey, K. K.; Ghosh, M. Understanding the effect of an anionic side-chain on the nuclear spin dynamics of a polysaccharide. *Cellulose* **2022**, *29*, 1381−1392.
(54) Dey, K. K.; Ghosh, M. Understanding the effect of deacetylation on chitin by measuring chemical shift anisotropy tensor and spin lattice relaxation time. *Chem. Phys. Lett.* **2020**, *738*, 136782.
(55) Dey, K. K.; Gayen, S.; Ghosh, M. Structure and dynamics of sodium alginate as elucidated by chemical shift anisotropy and site-specific spin−lattice relaxation time measurements. *Eur. Biophys. J.* **2021**, *50*, 963−977.

https://doi.org/10.1021/acsomega.3c03406
ACS Omega 2023, 8, 24093−24105

(56) Bhowal, R.; Balaraman, A.; Ghosh, M.; Dutta, S.; Dey, K. K.; Chopra, D. Probing Atomistic Behavior to Unravel Dielectric Phenomena in Charge Transfer Cocrystals. *J. Am. Chem. Soc.* **2021**, *143*, 1024−1037.
(57) Torchia, D. A. The measurement of proton-enhanced carbon-13 T1 values by a method which suppresses artifacts. *J. Magn. Reson.* **1978**, *30*, 613−616.
(58) Van Rossum, B. J.; Forster, H.; De Groot, H. J. M. High-Field and High-Speed CP-MAS 13C NMR Heteronuclear Dipolar Correlation Spectroscopy of Solids with Frequency-Switched Lee−Goldburg Homonuclear Decoupling. *J. Magn. Reson.* **1997**, *124*, 516−519.
(59) Al-Omar, M. A. Chapter 6 Ofloxacin. *Profiles Drug Subst., Excipients, Relat. Methodol.* **2009**, *34*, 265−298.
(60) Levitt, M. H.; Madhu, P. K.; Hughes, C. E. Cogwheel phase cycling. *J. Magn. Reson.* **2002**, *155*, 300−306.
(61) Ivchenko, N.; Hughes, C. E.; Levitt, M. H. Application of cogwheel phase cycling to sideband manipulation experiments in solid-state NMR. *J. Magn. Reson.* **2003**, *164*, 286−293.
(62) Herzfeld, J.; Berger, A. E. Sideband Intensities in NMR Spectra of Samples Spinning at the Magic Angle. *J. Chem. Phys.* **1980**, *73*, 6021−6030.
(63) Asakawa, N.; Kameda, T.; Kuroki, S.; Kurosu, H.; Ando, S.; Ando, I.; Shoji, A. Structural Studies of Hydrogen-bonded Peptides and Polypeptides by Solid-state NMR. *Annu. Rep. NMR Spectrosc.* **1998**, *35*, 55−137.
(64) Holstein, J. J.; Luger, P.; Kalinowski, R.; Mebs, S.; Paulman, C.; Dittrich, B. Validation of experimental charge densities: refinement of the macrolide antibiotic roxithromycin. *Acta Crystallogr., Sect. B: Struct. Sci.* **2010**, *66*, 568−577.
(65) Gorman, E. M.; Samas, B.; Munson, E. J. Understanding the Dehydration of Levofloxacin Hemihydrate. *J. Pharm. Sci.* **2012**, *101*, 3319−3330.
(66) Wei, N.; Jia, L.; Shang, Z.; Gong, J.; Wu, S.; Wang, J.; Tang, W. Polymorphism of levofloxacin: structure, properties and phase transformation. *CrystEngComm* **2019**, *21*, 6196−6207.
(67) Sakore, S.; Choudhari, S.; Chakraborty, B. Biowaiver monograph for immediate release solid oral dosage forms: Ofloxacin. *Int. J. Pharm. Pharm. Sci.* **2010**, *2*, 156−161.

https://doi.org/10.1021/acsomega.3c03406
ACS Omega 2023, 8, 24093−24105